Developments and Upgrades of Storage Ring

Orbit Stability

In 2005, the entire user operation was performed in the top-up mode. Accordingly, the beam orbit stability was excellent compared with the previously used decay mode. The remaining problem is the relatively large orbit variation over a long period, which we will mention below.

Low emittance optics have not small linear dispersion at the source points of insertion devices (IDs) and, hence, the photon axes of the ID beamlines suffer serious orbit variation by earthquakes. The dedicated feedback system, which precisely detects the circumference variation and adjusts the RF frequency of the RF acceleration with a resolution of 0.01 Hz, is under development.

To suppress the orbit drift at the restart of user operation, we have investigated the mechanical stability of beam position monitors (BPMs). The stability during beam operation was measured using several inductive displacement sensors. The measurements show that the displacements in the top-up operation are less than 2 μm, including a measurement error. However, they also show that at the restart of operation, the maximum horizontal and vertical drifts reach ~12 and ~7 μm, respectively. The stored electron beam directly and indirectly heats the vacuum chamber and, hence, a thermal expansion of the aluminum vacuum chamber occurs depending on the beam filling condition and stored current. The estimated thermal expansion of the chamber where a BPM is mounted well explains the measured data. To reduce the thermal expansion, the flow rate of the cooling water fed to the chamber was increased four times, which resulted in the horizontal and vertical displacements decreasing to a half of the previous values, ~7 and ~3 μm, respectively. Figure 1 shows the horizontal and vertical displacements of two BPMs during user operation after the cooling improvement.

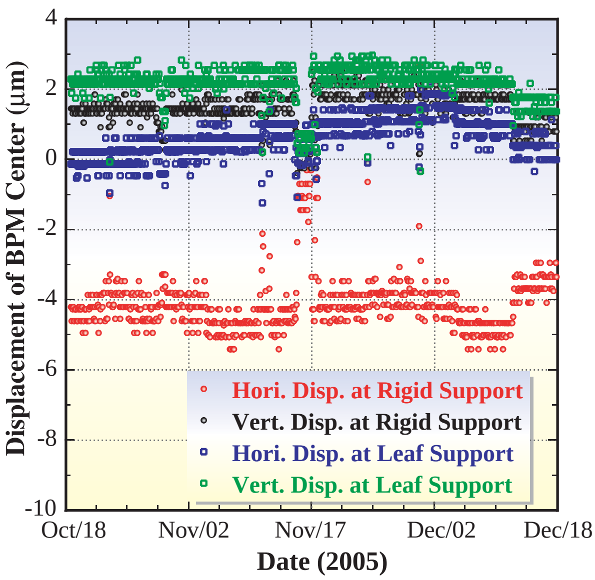

Fig. 1. Long-term stability of two BPM mechanical positions with different support methods. The red and black circles represent the horizontal and vertical displacements for the BPM fixed with the rigid support, respectively. The blue and green squares represent the horizontal and vertical displacements for the BPM fixed with the leaf support, respectively.

After introducing the top-up operation, the one-day orbit variation appears clearly in the variation of the field strengths of high-resolution steering magnets (HRSTs) used in the periodic closed orbit distortion (COD) correction. We have thus been investigating the mechanism of this pseudo-periodic variation. By analyzing the setting current data (corresponding to the field strength) of HRSTs, we have recently identified the error source locations, each of which has a tunnel or a trench under the floor of the machine tunnel. We selected one source location where the SSBT tunnel runs under the floor and carried out the systematic measurement of, for example, environmental parameters, the deformation of the girder, and the displacements of the magnets on the girder. At present, the results suggest an interesting mechanism: The fluctuation of AC voltage varies the air flow rate from the fan-coil unit and this flow rate change causes the deformation of the machine tunnel. The local deformation of the floor causes two central focusing quadrupole magnets on the second girder of cell 44 to incline. Figure 2 shows the correlation among these parameters. To clarify the mechanism, the systematic measurements and investigation are being continued.

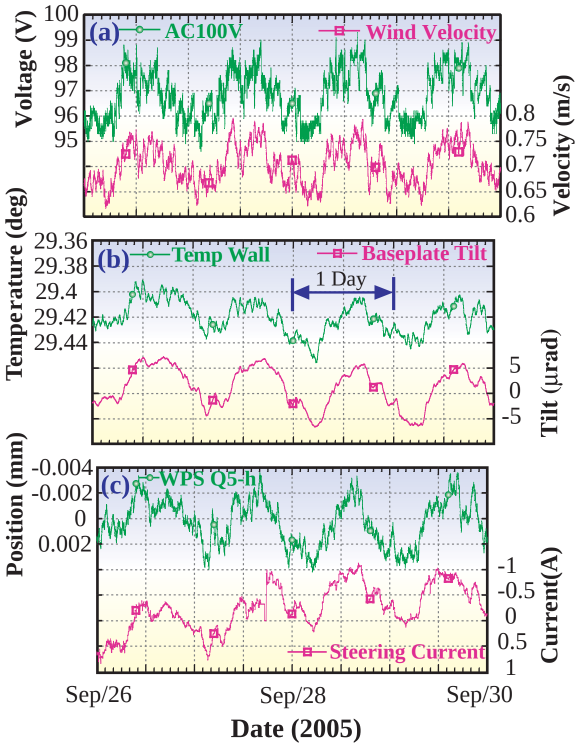

Fig. 2. Deformation of machine tunnel at cell 44 by variation of AC voltage. **(a)** correlation between AC voltage of fan-coil unit at cell 44 and velocity of circulating air from fan-coil unit, **(b)** correlation between surface temperature of inner wall of machine tunnel (experimental hall side) and tilt of central base plate at cell 44, and **(c)** correlation between horizontal displacement of QF5 at cell 44 and current of HRST at cell 43.

Top-up Operation

Top-up operation with a low emittance electron beam was started in September 2005 [1]. From the measurements of the photon fluxes of monochromatized X-rays emitted from the long undulator at BL19LXU, it is found that the peak flux in the new operation is 2.7 times larger than that in the previous operation, which is well explained by the calculation based on the design. The brightness enhancement is greatly beneficial for user experiments, and not only reduces the measurement time but also improves the data accuracy. A method of reducing the emittance employed at the SPring-8 storage ring is explained in ref. [2]. The emittance is reduced by breaking the achromatic condition imposed on the original double-bend achromat optics. In this situation, the dispersion function is nonzero at IDs and the energy spread of an electron beam enlarges the lateral beam extent through the dispersion function. The dispersion function is then optimized so that the phase space volume including the effect of the energy spread at a straight section of an ID takes the minimum value, as shown in Fig. 3.

Operation with a low emittance electron beam was first available for user experiments in November 2002 [3]. Although the low emittance electron beam provided brilliant X-rays, an extremely short beam lifetime due to the high electron density caused a significant variation in X-ray intensity, which disturbed precise experiments. First of all, the enormously short lifetime decreases the integrated or average brilliance against the expected end of the low emittance optics. Moreover, since the aborted electron beam damaged part of the vacuum chamber at the beam injection section, operation with the low emittance electron beam was suspended in October 2003. By improving the design of the vacuum chamber and introducing top-up injection [4-9], the problems for stable operation were resolved.

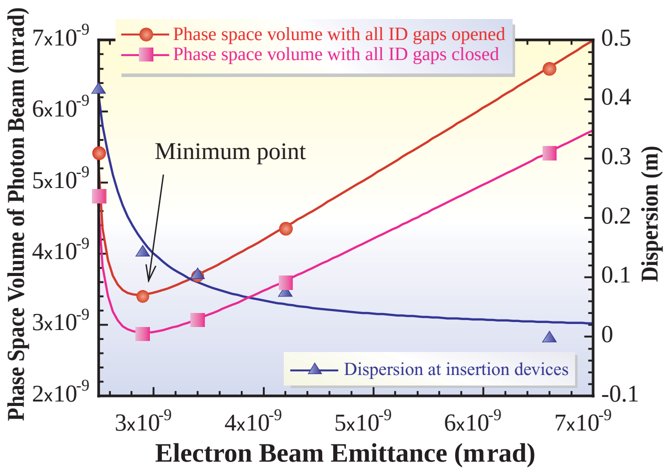

Fig. 3. Dependence of phase space volume of photon beam (vertical axis left) and dispersion at each insertion device (vertical axis right) on electron beam emittance (horizontal axis).

Development of New BPM Electronics

New signal processing electronic circuits for SPring-8 storage ring BPMs are under construction to improve the performance of the BPMs: faster measurement with the same level of resolution or better resolution with the same measurement time as the presently used electronics. The present circuits are scheduled to be replaced with the new circuits during the summer shutdown of 2006.

The present circuit was optimized for small signals so that the orbit could be measured with the small amount of stored electrons at the commissioning stage. Larger signals than those corresponding to 1 mA of stored current are attenuated before input to the RF amplifier stage to avoid nonlinear effects induced by large signal amplitudes. However, the signal-to-noise ratio (S/N) cannot be improved for a stored current larger than 1 mA, in spite of the increase in signal strength, because the input signal level to the RF amplifier is kept constant for a signal larger than the signal corresponding to 1 mA of stored current.

The design of the new circuits was optimized for 100 mA of stored current. The typical signal strength of 100 mA of stored current at the circuit input is -20 dBm for the single 508.58 MHz spectral component. 508.58 MHz is the acceleration RF frequency and also the detection frequency of the BPM signal processing circuits. The target resolution is in the sub-µm range; the stability must also be in the same range. A multiplexing method was employed to fulfill the stability condition. Ambient temperature stabilization is also planned and will employ a temperature controlled cabinet enclosure for stability, so the effects of temperature dependent drift are expected to be small. One set of the circuit consists of the following components: a filter-switch module to attenuate unnecessarily high frequency components for the protection of switching elements and to multiplex signals from BPM electrodes, an RF amplifier module having a narrow-band band-pass filter with a 3-dB bandwidth of less than 400 kHz at the center frequency of 508.58 Mhz, a mixer to down convert the signal to a 250 kHz IF (intermediate frequency) signal, an IF amplifier to adjust the signal level for the subsequent ADC, an ADC module to sample and digitize the IF signal, and a DSP module as a VME board to calculate the beam positions. Figure 4 shows a simplified block diagram of one set of the new circuits. One of the features of the new circuit is that the IF signal is sampled with a 16-bit 2MSPS ADC to achieve a good linearity. Most of the nonlinearity of the present circuit comes from the demodulation stage. Since the nonlinearity is the dominant factor in the stored current dependence of the measured position data, an improvement of the stored current dependence is expected to be achieved by the IF sampling method.

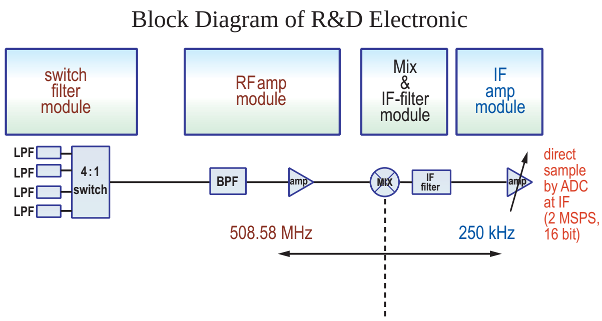

Fig. 4. Simplified block diagram of new electronics.

An example of data taken with a prototype of the new circuits is shown in Fig. 5. Data taken from two kinds of signal sources are compared: one is a signal generator with a CW output and the other is the beam signal. The signal generator output was divided by four, input to the circuit and processed. The processed signals were converted to the equivalent beam position data. The data taken with the signal generator show that the resolutions of 1 µm pk-pk (less than 0.3 µm in standard deviation) in both the horizontal and vertical directions are expected. However, data taken with actual beams show resolutions of 15 µm pk-pk (3.5 µm in standard deviation) in the horizontal direction and 10 µm pk-pk (1.9 µm in standard deviation) in the vertical direction, which are several to ten times worse than expected from the signal generator data. The discrepancy is due, at least partially, to the motion of the beam. The realization of the full performance of the BPM system requires the separation of the effect of the beam motion on the position measurements. Further study should be carried out to achieve the expected sub-µm resolution for the actual beam.

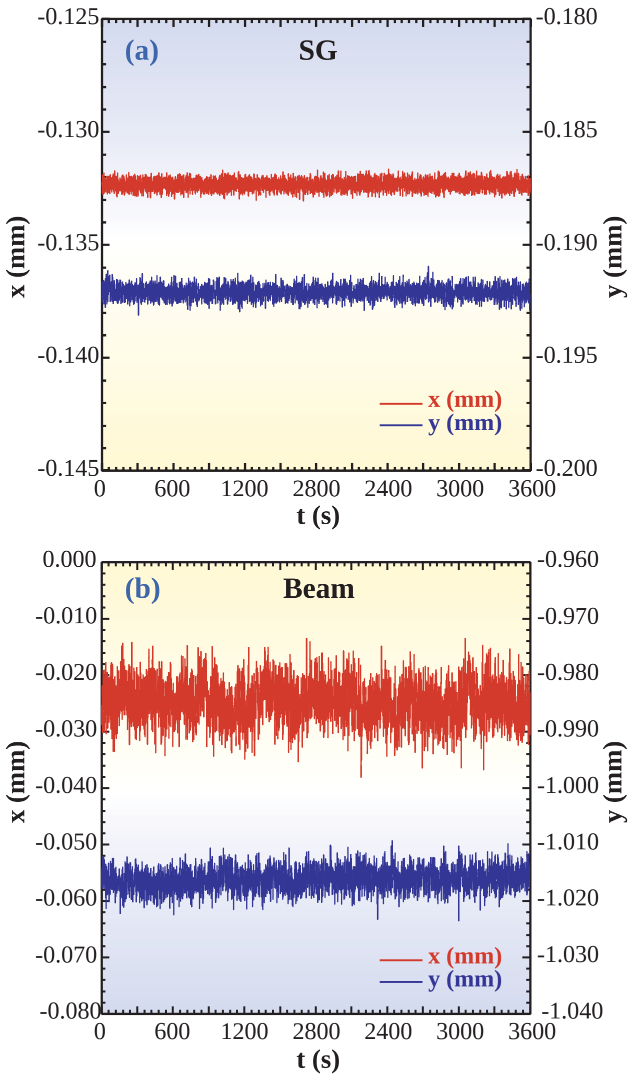

Fig. 5. Example of position data taken with prototype of new electronic circuits. **(a)** The signal source is a signal generator. **(b)** The signal source is the beam.

horizontal and vertical beam instabilities using one single loop; one diagonal pair of electrodes at a skewed position as a beam position monitor, one stripline at a skewed position as a kicker to detect and kick the beam horizontally and vertically, and one feedback processor, as shown in Fig. 6. This makes feedback systems easy to tune and highly cost-effective.

The single-loop two-dimensional feedback with new SPring-8 feedback processors is employed by Photon Factory at KEK and Taiwan Light Source at NSRRC, Taiwan, and are in user operation.

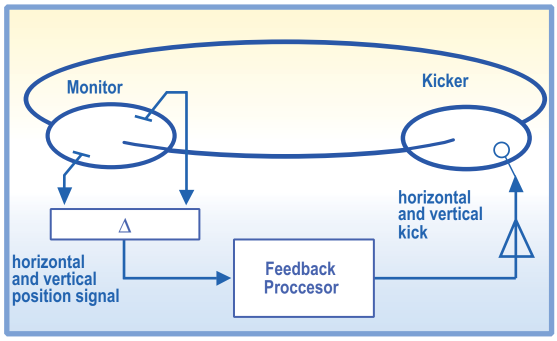

Fig. 6. Single-loop two-dimensional feedback using new SPring-8 feedback processor.

Improvement of Bunch-by-bunch Feedback

A new bunch-by-bunch feedback processor has been developed for planned advanced operation modes of the SPring-8 storage ring and for the ease of tuning of the system by simplifying the architecture and making the system USB-controllable with a Linux-based PC. The system can also handle two 20-tap FIR filters or one 50-tap FIR filter that enable single-loop two-dimensional transverse feedback with a newly developed method for the calculation of FIR filter coefficients. This scheme can suppress

Development of Accelerator Diagnostics Beamlines

A schematic layout of the accelerator diagnosis beamline I (BL38B2) is shown in Fig. 7. The light source of the beamline is a bending magnet, and synchrotron radiation (SR) in a wide spectral range from visible light to X-rays can be utilized. Visible SR is used for the diagnostics of the longitudinal properties of the source electron beam, such as bunch length and bunch purity [10]. X-rays are used for emittance diagnostics of the electron beam using an X-ray beam imager (XBI) based on a Fresnel zone plate (FZP) and an X-ray zooming tube [11].

The accelerator diagnosis beamline II (BL05SS) is the second diagnostics beamline that is under construction. It has a straight section of the storage ring for an ID. The beam diagnostics and

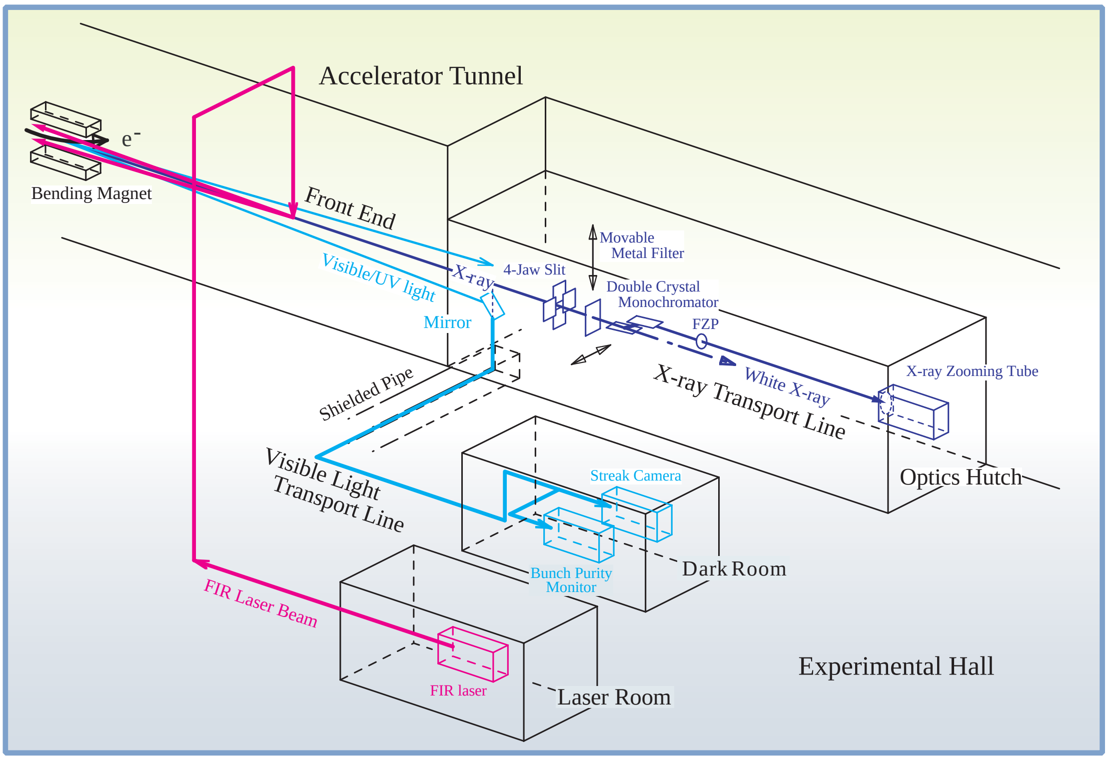

Fig. 7. Schematic view of accelerator diagnosis beamline I (BL38B2).

R&Ds of accelerator components are planned utilizing SR from the ID. The ID was developed and installed in the accelerator tunnel of the storage ring in 2005. The magnet array presently mounted on the ID is of the multipole wiggler (MPW) type and is designed to produce high-power SR. Studies of radiation damage to accelerator components and the development of high-thermal-load components such as photon absorbers are planned, utilizing SR from the MPW. A compact photon absorber developed to withstand the high heat load of the SR from the MPW was installed in the front-end in 2005. Designs of vacuum components for the X-ray transport line to be installed in the radiation shielding hutches of the diagnosis beamline II are in progress. For example, a differential pumping system was developed, which is necessary to connect the ultra high vacuum section in the range of 10^{-8} Pa and the low vacuum section in a range of 10^{-4} Pa directly without any vacuum partitions such as beryllium windows.

The study of the production of γ-ray photons in the energy range of 10 MeV is in progress at BL38B2 and BL05SS. The MeV γ-rays are generated by the backward Compton scattering of optically pumped far-infrared laser photons from 8 GeV electrons in the storage ring [12].

Improvement of Pressure Measurements

The abnormal actions of a Bayerd-Alpert type ionization gauge were observed. Gauges on the downstream end of the straight section chamber and on the crotch chamber are installed very close to the photon absorber. Therefore, these gauges are influenced by photoelectrons and radiation from the photon absorber. By precise measurement, three origins of abnormal action were confirmed as follows: the effects of (i) radiation on the gauge head, (ii) electron inflow on the gauge head, and (iii) radiation on gauge cable. (i) was also reported at ELETTRA, Italy [13]. (ii) is a well-known effect in accelerators. (iii) occurred owing to radiation induced current, and in this case the reading pressure was lower than the actual pressure. The following measures were made: (i) the shielding of the gauge head's casing with lead of 3 mm thickness, (ii) the additional installation of a U tube or a permanent magnet upstream of the gauge head port, and (iii) the replacement of damaged cable with new cable, and the shielding of cables with lead tube of 3 mm thickness.

Figure 8 shows the normalized pressure rise (ΔP/I) and the product of the beam current (I) and beam lifetime (τ) as a function of the beam dose. I • τ increased with the integration of beam dose. SC1 shows ΔP/I at the middle of the straight section where the amount of radiation is very low. AB3 and CR1 show ΔP/I near the photon absorber. ΔP/I of SC1 decreased constantly in proportion to (beam dose)$^{-0.8}$. On the other hand, ΔP/I of AB3 and CR1 decreased negligibly after 10 Ahr of beam dose. ΔP/I of AB3 and CR1, however, decreased rapidly after 1014 Ahr of beam dose, because of the above-mentioned measures. ΔP/I of AB3 and CR1 were almost equal to that in SC1.

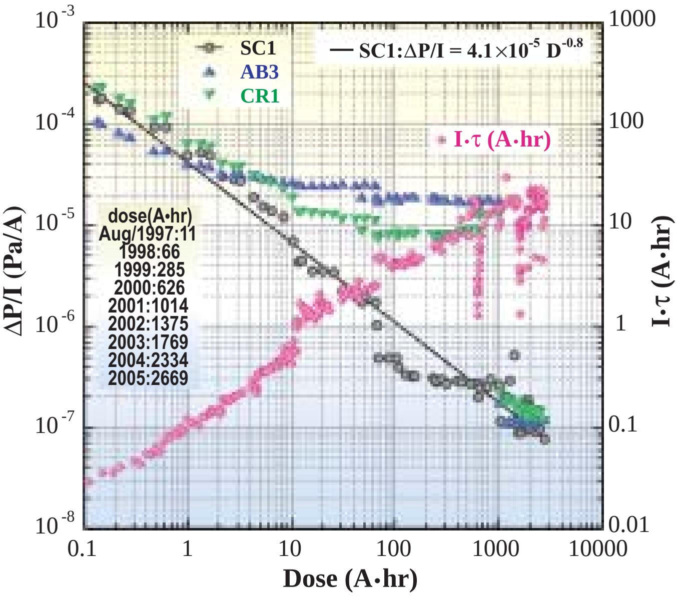

Fig. 8. Normalized pressure rise (ΔP/I) and product of beam current (I) and beam lifetime (τ) as a function of beam dose.

Study on Local Modification of Optics at Long Straight Section for Installing Superconducting Wiggler

The generation of high-energy SR in the MeV range using a 10 T superconducting wiggler (SCW) has been studied. High-energy SR from the SCW can be applied to new research fields such as nuclear astrophysics experiments, etc. [14-18].

To make use of the SCW in user operation at 100 mA, we have to solve the problems of high heat load, radiation shielding, non-negligible effects on the stored beam, etc. For example, when the SCW is excited in the storage ring, the emittance changes with the values of the horizontal betatron function and dispersion function at the place of installation of the SCW. A drastic increase in the emittance can be avoided by changing the storage ring optics locally and making a low-beta insertion at the SCW. A possible place for installation is one of four magnet-free long straight sections (LSSs) of about 30 m. In Fig. 9, we show an example of the local modification of optics. If we make such a local modification of optics, the periodicity of cell structure, especially of the sextupole field distribution, is broken and the symmetry of the ring becomes low. As a result, the dynamic aperture becomes narrow, and the beam injection efficiency and beam lifetime deteriorate.

To recover the periodicity of cell structure and hence the dynamical stability, we developed a method of “counter-sextupoles.” In this method, additional sextupole magnets are placed within the matching section to cancel the nonlinear kick due to the sextupole magnets for local chromaticity correction, which are located in the arc of the matching section. The betatron phase between the counter-sextupoles and the sextupoles for local chromaticity correction is chosen to be as close as possible to π to make such a cancellation. To check the effectiveness of this scheme, we installed additional quadrupole and sextupole magnets in one of the four LSSs, as shown in Fig. 9. We measured beam parameters for the modified optics and checked the effectiveness

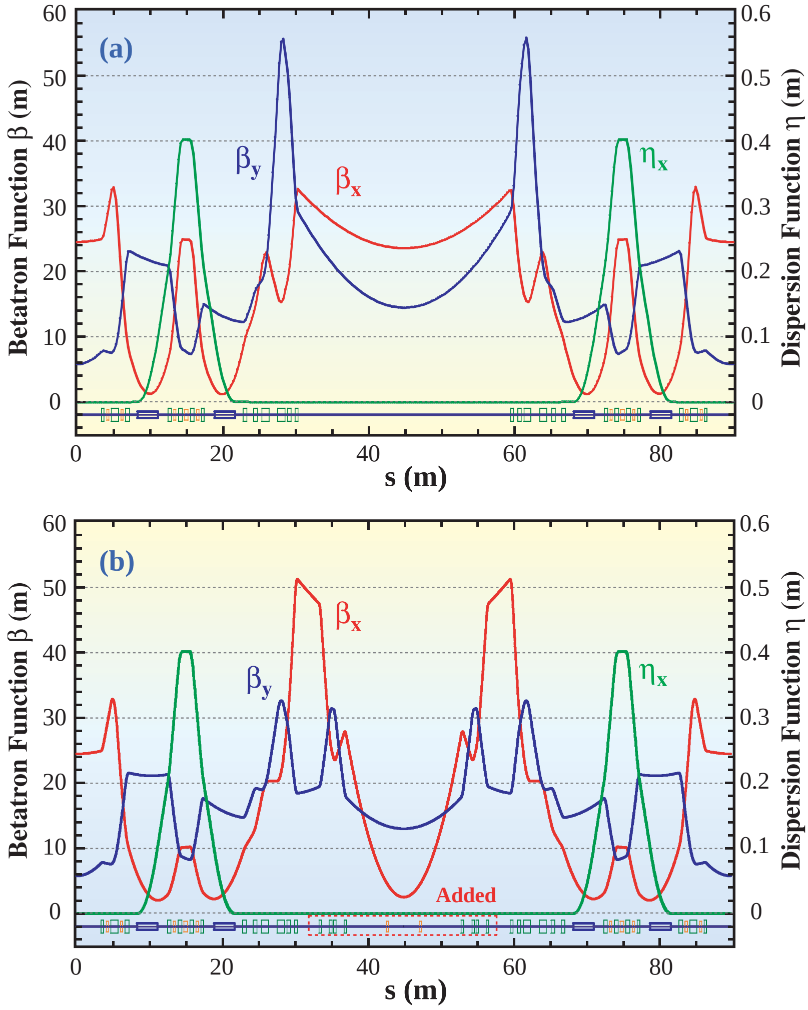

Fig. 9. Optics of matching section **(a)** before and **(b)** after local modification. Bending, quadrupole and sextupole magnets are shown by blue, green and orange rectangles, respectively.

of the above scheme. We, however, could not fully recover the degree of stability because the rest of the LSS's were remained unchanged and the kick due to the sextupole magnets was not canceled in these sections. We are now planning to install counter-sextupoles in all four of the LSSs and this will improve the beam performance in routine user operation. It is also expected that, with this scheme of counter-sextupole independent tuning of local optics at each LSS, it will become possible to insert devices other than the SCW.

Developments and Upgrades of Booster Synchrotron

Beam Storage Operation of Booster Synchrotron

To improve the performance of the booster synchrotron, especially for the high duty operation of top-up injection, it is important to understand the detailed characteristics of the booster synchrotron. Beam storage operation is effective for measuring various parameters, such as HOM in the RF cavity at 1 GeV, COD at each energy, and emittance at each energy, which are difficult to measure in normal energy ramping operation.

For a test operation of the beam storage, it was necessary to modify the timing system. In booster operation, all pulsed magnets are operated at 1 Hz. Other magnets and RF acceleration voltage are operated ramping up and down at 1 Hz. For storage operation, the timing system was modified to stop its chain at the desired time. In this test operation, a beam lifetime of 2.7 hours at a stored beam current of 8.6 mA was achieved.

Measurement of Demagnetization of Undulator Magnet

Permanent magnets are the main components of undulators. The demagnetization of the magnets in a highly radioactive environment is a serious problem. For the experimental use of the SPring-8 booster synchrotron, instead of beam injection into the storage ring, we investigated the demagnetization of an undulator magnet by irradiating the magnet with the electron beam to in January 2005.

A 40-mm-thick copper block was placed in front of the magnet and the electron beam was irradiated onto the block. The electron beam irradiation was carried out at the beam dump of the booster synchrotron. After the beam irradiation, the magnetic field distribution of the undulator magnet was measured using a Hall probe. The electron beam was injected into the target Cu block, passing through a 1-mm-thick aluminum vacuum window and a fluorescence screen for beam position monitoring. The electron dose was monitored by DCCT in the booster synchrotron.

The repetition rate of beam irradiation was 1 Hz, and the beam irradiation dose was 1.4×10^{15} electrons for each sample magnet. Various beam energies were used: 4 GeV, 6 GeV and 8 GeV, respectively. The result of the experiment, the beam energy dependence of demagnetization, was observed. Data analysis is now in progress.

Developments and Upgrades of Linac

Beam Stabilization [19]

The SPring-8 linac has been improved to realize stable top-up injection into the SPring-8 and the NewSUBARU storage rings. A long-term beam energy instability of 0.02% rms was achieved by the following stabilizations (1998 - 2005): RF amplitude and phase stabilization, the synchronization of beam timing and the linac's 2856 MHz RF, and the installation of an energy compensation system (ECS). Beam feedback controls compensate for the residual long-term variation of beam trajectory and energy.

Air temperature fluctuations in the linac klystron gallery have reappeared since 2002 because of the electric power saving of the linac. The temperature variations have resulted in RF phase fluctuations in a 100-m-long waveguide that drives eleven klystrons. The improvement of an air conditioning system has stabilized the temperature fluctuations less than 1ºC, as shown in Fig. 10. In addition, the long waveguide is covered with thermal insulation and warm water (27±1ºC) is circulated in pipes inside the cover. The air temperature fluctuations inside the insulation have been consequently reduced to 0.23ºC.

To improve the long-term stability, we introduced the following feedback controls: (i) beam position stabilization at three beam transport

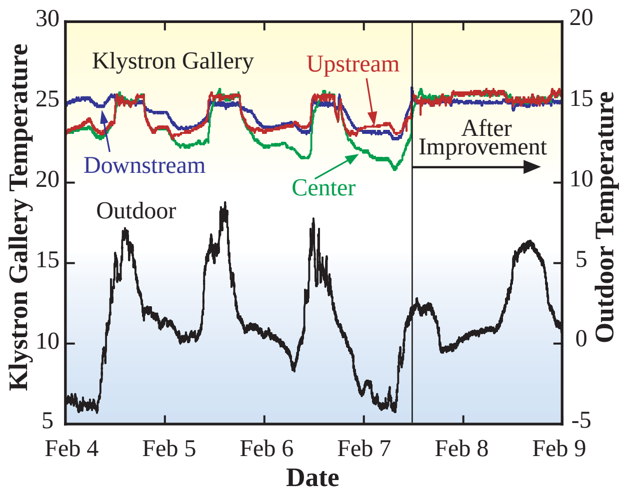

Fig. 10. Variations of klystron gallery temperatures before and after improvement.

lines, and (ii) beam energy stabilization by adjusting the ECS. Beam position control is carried out at the following three points in the linac: (i) a drift space in the injector, (ii) the drift space of a transport line to the NewSUBARU storage ring, and (iii) a transport line between the ECS and a bending magnet downstream. These straight parts respectively contain two sets of steering magnets upstream and two sets of BPMs downstream. The control program adjusts the steering magnets and maintains beam positions within the position window at reference BPMs. The position window was determined to be ±30 μm, which is nearly double the standard deviation of the measured values.

Beam energy is stabilized as follows: it is measured by BPMs installed at the dispersive sections of the beam transport line to the NewSUBARU or to the booster synchrotron. The program adjusts the RF phase of the ECS so that energy error remains within the energy window of ±0.03%.

Development of Photocathode RF Gun

A study of a photocathode RF gun, which is expected to be a highly qualified electron beam source for producing future X-ray light sources, has been in progress since 1996 at SPring-8. We have promoted the development of basic technologies especially for producing low emittance beams with a single-cell type RF gun [20]. The next step in this R&D project is to verify the beam performance, particularly the beam emittance, in the higher beam energy region because a single-cell cavity can only accelerate beams up to 4.1 MeV and the emittance can easily grow in this energy region. To enhance the beam energy, a 3-m-long traveling wave structure has been added after the RF gun, as shown in Fig. 11 [21], and thus the approved maximum beam energy has been increased from 4.1 MeV to 30 MeV. At present, the beam emittance is evaluated by the variable quadrupole magnet method, which often underrates the actual emittance. An emittance measurement system based on the double slit scanning method, which generally enables a more accurate emittance evaluation, is now under construction.

An electron bunch having a uniform density distribution is expected to minimize the nonlinear space charge effect, which causes the emittance growth. Hence, we have developed optical systems to control the spatial and temporal shapes of laser light pulses to realize such ideal charge distributions. We employed a computer-aided deformable mirror as a spatial shaper [22]. This deformable mirror consists of 59 small hexagonal mirrors with center-to-center distances of 1.75 mm. A control voltage between 0 and 250 V, in increments of 1 V, is applied to each mirror, making it possible to shape any laser spatial profile, with a total of 25059 (~10141) forming possibilities. Thus, this spatial shaping method needs a sophisticated algorithm to control the deformable mirror. As a result, the laser profile on the cathode surface was spatially shaped to have a quasi-flattop profile (right-hand side of Fig. 12). The laser beam diameter was estimated to be 1.0 mm.

The copper cathode was illuminated by this shaped laser pulse at normal incidence. The measured horizontal normalized emittance of the accelerated beam was 1.74 π mm·mrad at its minimum with a net charge per bunch of 0.09 nC/bunch [22].

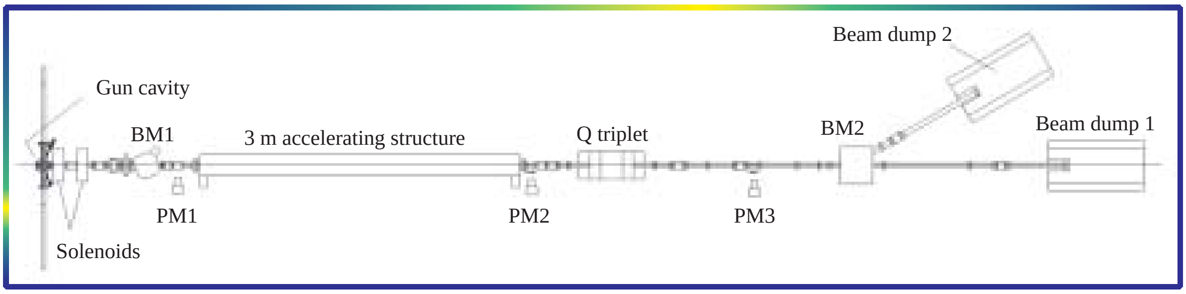

Fig. 11. Layout of 30-MeV linac with photocathode.

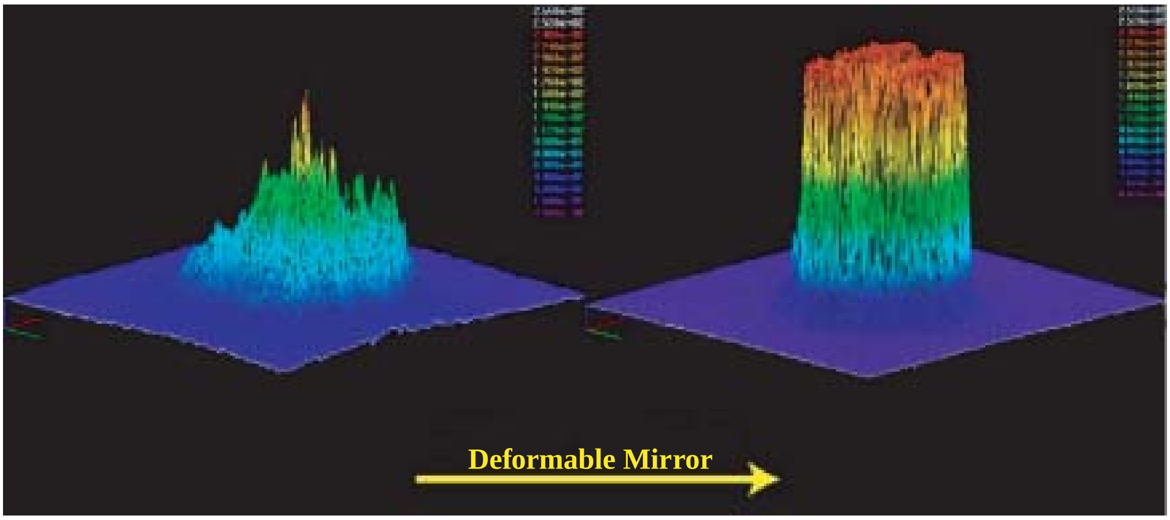

Fig. 12. Spatial shaping results using deformable mirror and genetic-algorithm-based optimizations.

Haruo Ohkuma*, Hiroto Yonehara,
Hirofumi Hanaki and Noritaka Kumagai

SPring-8 / JASRI

*E-mail: ohkuma@spring8.or.jp

References

[1] H. Tanaka *et al.*: to appear in Proc. EPAC06, Edinburgh, UK.
[2] H. Tanaka *et al.*: Nucl. Instrum. Meth. A **369** (1996) 312.
[3] M. Takao *et al.*: to appear in Proc. APAC04, Gyeongju, Korea.
[4] H. Tanaka *et al.*: Proc. of EPAC 2004, Lucerne, Switzerland, 222.
[5] M. Takao *et al.*: Proc. of EPAC 2004, Lucerne, Switzerland, 417.
[6] K. Fukami *et al.*: to appear in Proc. of APAC 2004, Gyeongju, Korea.
[7] T. Ohshima *et al.*: Proc. of EPAC 2004, Lucerne, Switzerland, 414.
[8] H. Tanaka *et al.*: Proc. of EPAC 2004, Lucerne, Switzerland, 1330.
[9] H. Tanaka *et al.*: Nucl. Instrum. Meth. A **539** (2005) 547.
[10] K. Tamura *et al.*: Proc. 1st Annual Meeting of Particle Accelerator Society of Japan and Proc. 29th Linear Accelerator Meeting, Funabashi, Japan, 2004, p.581.
[11] S. Takano *et al.*: Nucl. Instrum. Meth. A **556** (2006) 357.
[12] H. Ohkuma *et al.*: to appear in Proc. EPAC06, Edinburgh, UK.
[13] J. Miertusova: Vacuum **51** (1998) 61.
[14] H. Yonehara *et al.*: SPring-8 Internal Report B2004-001 (2004) (in Japanese).
[15] H. Utsunomiya *et al.*: Nucl. Phys. A **738** (2004) 136.
[16] H. Utsunomiya *et al.*: Nucl. Instrum. Meth. A **538** (2005) 225.
[17] A. Ando *et al.*: J. Synchrotron Rad. **3** (1996) 201.
[18] D.A. Gryaznykh *et al.*: Nucl. Instrum. Meth. A **448** (2000) 106.
[19] H. Hanaki *et al.*: Nanobeam2005, Uji, Japan.
[20] H. Dewa *et al.*: Proc. ICFA Workshop “The Physics and Applications of High Brightness Electron Beams”, Sardinia, Italy, 2002, p.28.
[21] T. Taniuchi *et al.*: FEL’04, Trieste, Italy.
[22] H. Tomizawa *et al.*: FEL’05, Stanford, USA.

Impacts of the Top-up Operation to SR experiments

Of particular desire for synchrotron radiation (SR) experiment user is to attain a stable and no time decay X-ray beam. The top-up operation in SPring-8 has been realized to bring great advantages for user experiments.

The merits of the top-up operation for SR experiments are summarized as follows: (a) Increase in time averaged photon flux: The top-up operation achieved an expected increase in total photon flux, which leads to a high counting statistic measurement due to constantly high beam intensity. In addition, a continuous operation without shut down for refilling beam current excluded not only a shut down time loss but also a time loss for the warm-up of optics. Consequently, for multi bunch experiments, the top-up operation provides about 1.5 times higher intensity measurement in total while for the single bunch experiment 3 times higher intensity were provided, since a preferential beam filling for the use of a single bunch has an electron with shorter lifetime than that in the case of multi-bunch filling. (b) Current stability within 0.1% fluctuation: The minimized current fluctuation of a stored beam leads to a constant heat load for optics including monochromators, which enables the achievement of a virtually absolute measurement with intensity monitor free. (c) No interruption by refilling of beam: The operation without shut down for electron refilling allows us planning of long time stable measurement.

Here, we describe the merit of the step-scan measurement in a diffraction experiment as an example. In the case of step-scan measurement, the time dependent decay and fluctuation of incident X-ray intensity were used to be corrected by monitoring incident X-ray intensity. However, the precise top-up operation succeeded in the elimination of ambiguity over the step-scan measurement caused by a data correction based on the monitored intensity at each measurement step. This enhances the data reliability of the diffraction experiment.

The diffraction data of amorphous silica measured at the high-energy X-ray diffraction beamline **BL04B2** with 61.6 keV high-energy X-rays is shown in Fig. 1. Since the scattered intensity drastically decreases with an increase in scattering angle as shown in this figure, it is necessary to obtain the correct intensity profile in the high-angle region to place the observed data on an absolute scale. To obtain the correct intensity profile of disordered materials up to large values of scattering vector Q, the measurement is performed using $\theta - 2\theta$ step-scans with an intrinsic Ge detector over a period of 4 – 12 hours. Therefore, the incident flux of photons should have a high stability for a long time scan over a wide range of Q values.

Figure 2 (a) shows high angle data of amorphous silica measured in the conventional non-top-up mode. Here, it can be seen that the difference in scattering intensity between the first and second scans is due to the fluctuation of the incident beam flux. On the other hand, the two intensity profiles measured in the top-up mode are nearly identical, as shown in Fig. 2 (b). Figure 2 (c) shows the difference in scattering intensity between the first and second scans. In the case of the top-up mode, the difference is almost equal to zero, which demonstrates that a heat load on the monochromator of BL04B2 remains equal to a steady value owing to the constant stored beam current of the storage ring.

To clarify the effect of the top-up operation on

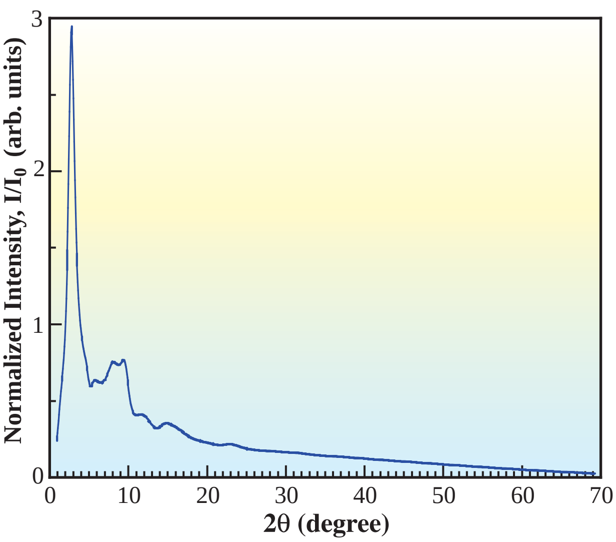

Fig. 1. X-ray diffraction pattern of amorphous silica.

the structural analysis of disordered materials, both of the diffraction data are normalized to the total structure factors $S(Q)$ and Fourier transformed to the total correlation functions in real space, $T(r)$. The $S(Q)$ of amorphous silica obtained in the top-up mode exhibits proper oscillations up to Q = 32 Å^{-1}, as shown in Fig. 3(a), whereas $S(Q)$ obtained in the conventional mode exhibits some artificial declination below $S(Q)$ = 1.0 in the high-Q region (Q > 20 Å^{-1}), which produce significant ripples in the correlation function, $T(r)$, as shown in Fig. 3(b), at r < 1 Å.

The top-up operation of SPring-8 allows us to very accurately measure diffraction data of disordered materials up to a high-Q. It is particularly well suited for detecting small differences in structure between two isotopically substituted amorphous samples such as an isotopic quantum effect in water [1].

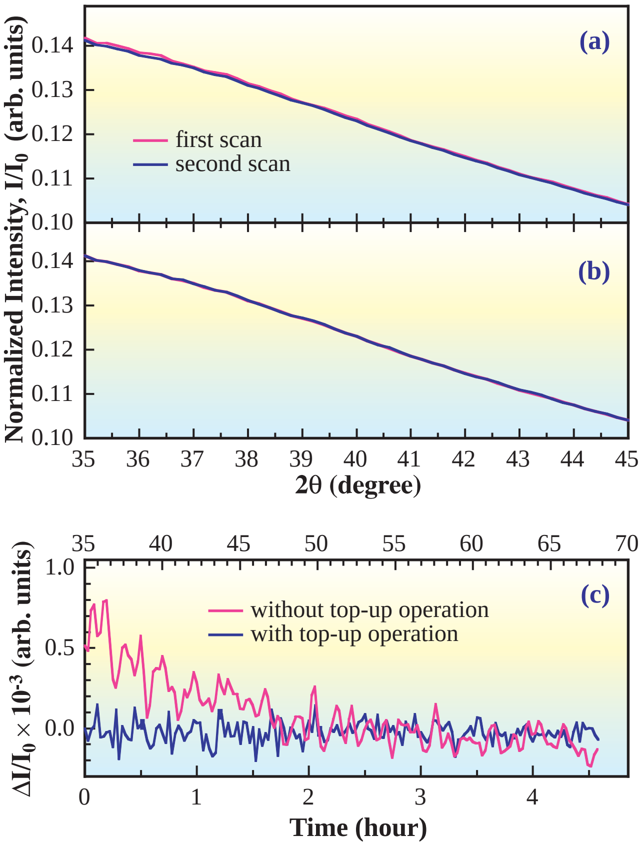

Fig. 2. X-ray diffraction patterns of amorphous silica without top-up operation **(a)** and with top-up operation **(b)**; the difference of first scan and second scan **(c)**.

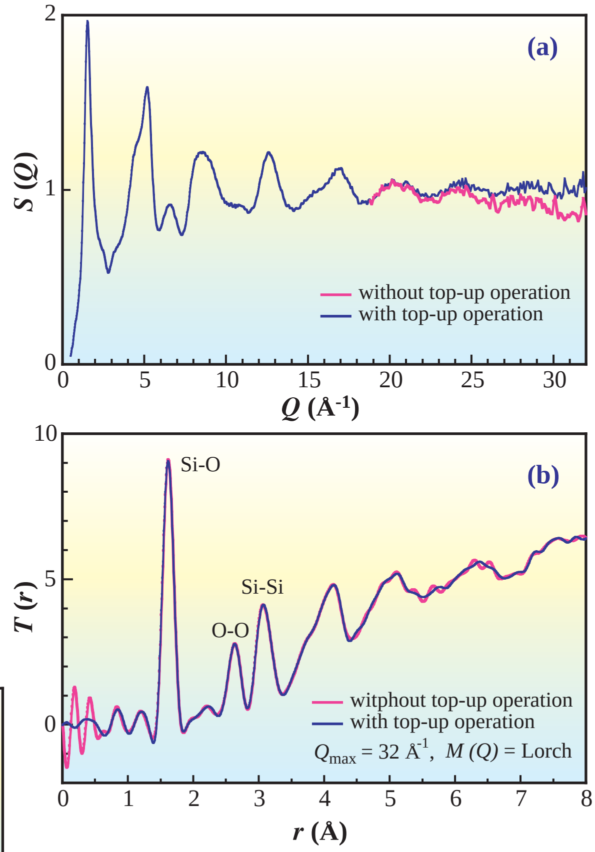

Fig. 3. Total structure factor $S(Q)$ **(a)** and total correlation function $T(r)$ **(b)** of amorphous silica.

Masaki Takata[a,b,*] and Shinji Kohara[a]

[a] SPring-8 / JASRI
[b] SPring-8 / RIKEN

*E-mail: takatama@spring8.or.jp

References

[1] R. Hart *et al.*: Phys. Rev. Lett. **94** (2005) 047801.